ACS APPLIED MATERIALS & INTERFACES

Research Article

www.acsami.org

Self-Assembled, Aligned ZnO Nanorod Buffer Layers for High-Current-Density, Inverted Organic Photovoltaics

Arun D. Rao,[†] Suresh Karalatti,[†] Tiju Thomas,*[,‡,§] and Praveen C. Ramamurthy*[,†]

[†]Department of Materials Engineering and [‡]Materials Research Center, Indian Institute of Science, Bangalore, Karnataka 560012, India

[§]Department of Metallurgical and Materials Engineering, Indian Institute of Technology, Madras, Chennai 600036, India

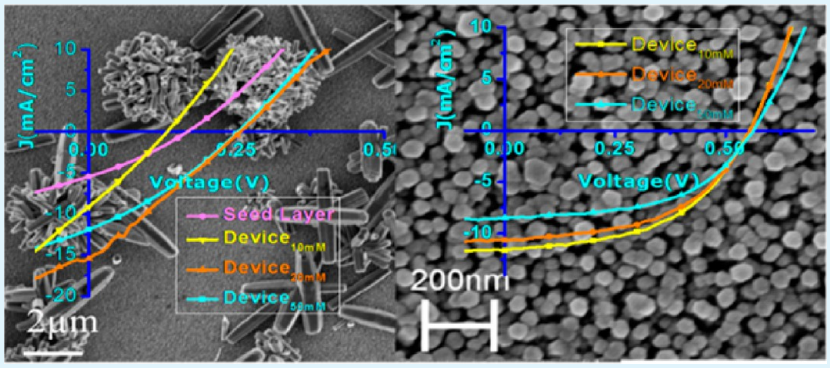

ABSTRACT: Two different soft-chemical, self-assembly-based solution approaches are employed to grow zinc oxide (ZnO) nanorods with controlled texture. The methods used involve seeding and growth on a substrate. Nanorods with various aspect ratios (1−5) and diameters (15−65 nm) are grown. Obtaining highly oriented rods is determined by the way the substrate is mounted within the chemical bath. Furthermore, a preheat and centrifugation step is essential for the optimization of the growth solution. In the best samples, we obtain ZnO nanorods that are almost entirely oriented in the (002) direction; this is desirable since electron mobility of ZnO is highest along this crystallographic axis. When used as the buffer layer of inverted organic photovoltaics (I-OPVs), these one-dimensional (1D) nanostructures offer: (a) direct paths for charge transport and (b) high interfacial area for electron collection. The morphological, structural, and optical properties of ZnO nanorods are studied using scanning electron microscopy, X-ray diffraction, and ultraviolet−visible light (UV-vis) absorption spectroscopy. Furthermore, the surface chemical features of ZnO films are studied using X-ray photoelectron spectroscopy and contact angle measurements. Using as-grown ZnO, inverted OPVs are fabricated and characterized. For improving device performance, the ZnO nanorods are subjected to UV-ozone irradiation. UV-ozone treated ZnO nanorods show: (i) improvement in optical transmission, (ii) increased wetting of active organic components, and (iii) increased concentration of Zn−O surface bonds. These observations correlate well with improved device performance. The devices fabricated using these optimized buffer layers have an efficiency of ∼3.2% and a fill factor of 0.50; this is comparable to the best I-OPVs reported that use a P3HT-PCBM active layer.

KEYWORDS: *inverted organic photovoltaics, self-assembly, zinc oxide nanorods, electron collectors*

INTRODUCTION

Organic photovoltaics (OPVs) are amenable to solution processing, which, in turn, makes these devices promising for low-cost solar energy conversion.[1−3] Cost-effective and scalable production of OPVs is possible because of the fact that large-scale fabrication of these devices is possible using printing or coating technologies. The relevant printing processes are very often done under soft-chemical (i.e., low-temperature) conditions; this aids in reduction of the energy payback times (EPBTs) associated with these devices. Development of suitable device fabrication processes can ensure further reduction in the EPBTs associated with these OPVs.[4] On the other hand, it is important to note that viability of OPVs is compromised because of poor device stability and low photovoltaic efficiencies. However, OPVs in the inverted configuration (i.e., I-OPVs) have demonstrated higher stability when compared to devices in the conventional configuration. Hence, the inverted device configuration, and associated fabrication processes (with possibly low carbon footprint and EPBT), are of current interest.[5]

From a materials technology point of view, the primary challenges (i.e., low efficiency and poor stability) associated with OPVs can be dealt with by replacing poly(3,4-ethylene dioxythiophene):polystyrene sulfonate (PEDOT:PSS) with metal oxides. The use of metal oxide nanostructures provides the combined advantage of high stability and large interfacial

Received: June 24, 2014
Accepted: September 5, 2014
Published: September 19, 2014

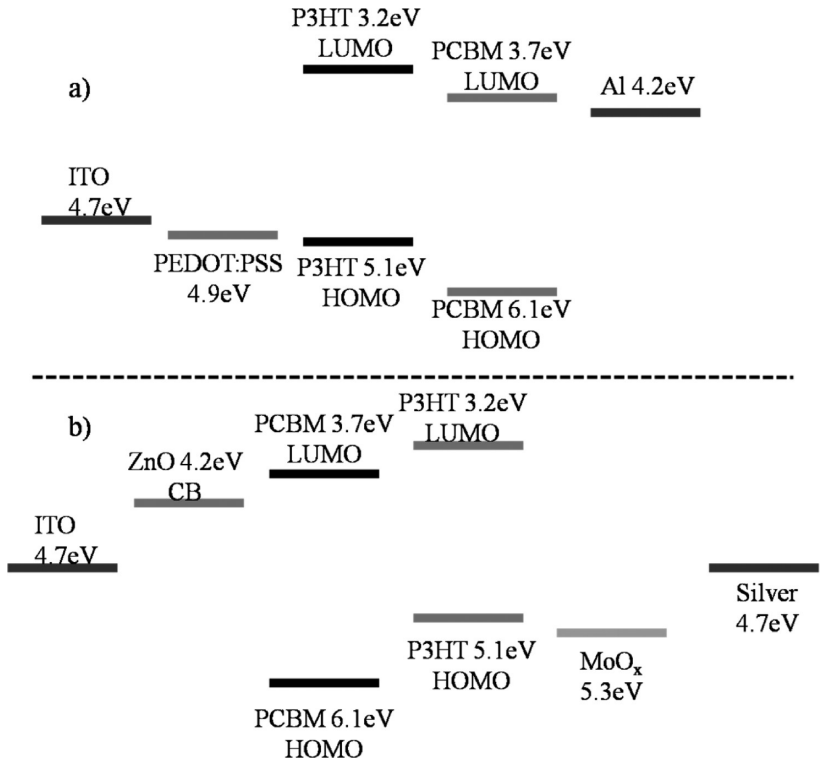

Figure 1. Energy band diagrams for (a) conventional organic photovoltaic (OPV) and (b) inverted organic photovoltaic (I-OPV).

area.[6] Similarly, in conventional OPVs, the air stability of the cathode can be improved by replacing Al (which has a low work function) with noble metals such as Au and Ag (Figure 1a). In the "inverted" configuration, wherein indium-doped tin oxide (ITO) is often used as the cathode,[7,8] various semiconductor nanostructures may be used instead. Among these semiconducting systems, ZnO-based systems are among the most promising (Figure 1b). This is because of the inherent stability of oxides,[9] and the ease with which it can be synthesized.[10−12] As electron collectors, one-dimensional (1D) ZnO nanostructures (i.e., nanorods) are attractive since they provide direct paths for charge transport, and also offer large interfacial area over which charge collection is made possible.[13−15] Hence, in this work, we focus on I-OPVs, wherein ZnO nanorods are used as electron collectors.[16]

In this work, we use self-assembly in order to obtain oriented ZnO nanorods. We use self-assembly because it has the natural advantage of being amenable to soft-chemical processing, which, in turn, reduces the EPBT associated with the device. However, there exist limitations to direct use of existing soft-chemical processes for semiconductor nanostructure growth. ZnO nanorods grown using these routes tend to have large defect (e.g., oxygen vacancies) densities.[17,18] Furthermore, minor changes in synthesis parameters result in substantial morphological heterogeneity.[19,20] This, in turn, impacts device performance. To enhance the technological viability of ZnO nanostructures, control over the defect densities and morphological heterogeneities is essential. It would be ideal if these controls could be achieved using soft and self-assembly based approaches, since fabrication based on these methods are scalable, cost-effective, and reduce the EPBT associated with I-OPV.

Among the techniques used for growing ZnO, evaporation and condensation processes are popular because of the high purity of the resultant product. Furthermore, gas-phase techniques allow control of intrinsic and extrinsic defect densities, to some extent. However, these techniques generally require high operating temperatures, which are in the range of ∼800−900 °C.[21−24] Hence, the commercial potential of gas-phase-grown ZnO nanorods is limited by the infrastructural and running costs associated with vapor deposition systems. In order to address this issue, it is reasonable to explore soft-chemical, solution-grown ZnO nanorods.[25−28]

In this work, a soft-chemical, aqueous route is used to grow ZnO nanorods of various aspect ratios. The ZnO nanorods are grown using two different approaches, one of which leads to better texture of these nanorods. The seeding process is the same in both approaches. In the growth processes reported, we notice that mounting of the substrate is a crucial parameter in elimination of lateral heterogeneities in the as-grown ZnO nanorods. In fact, in the second growth approach explored here, we get highly aligned ZnO nanorods, when the substrate is placed upside down and when it is in a state of suspension (i.e it must not be placed at the bottom of the chemical bath). Furthermore, the growth solution must be preheated and centrifuged appropriately for the second approach to be effective.

The effect of various other parameters such as concentrations of precursors and surfactants are studied. We also systematically investigate the impact of (i) different seed layers (zinc acetate dehydrate and zinc nitrate hexahydrate) and (ii) composition of the growth medium. When zinc nitrate hexahydrate is used as the precursor for seeding, orientations of the rods and packing density are found to be nonuniform. Whereas when the seed layer is grown using a zinc acetate dehydrate precursor, we achieved uniform, large-area, dense ZnO nanorods. Hence in the manuscript we mention only the zinc acetate route seeding

procedure. The optimized nanostructures are then incorporated as electron collectors in an I-OPV.

The structural and optical properties of the as-prepared and UV-ozone-treated ZnO nanorods are studied using scanning electron microscopy (SEM), X-ray diffraction (XRD), and ultraviolet−visible (UV-vis) absorption spectroscopy. Furthermore, the surface chemistries of structures grown are studied using contact angle measurements and X-ray photoelectron spectroscopy (XPS). The fabricated I-OPVs (which use ZnO nanorods as electron collectors) are characterized using a solar simulator.

2. EXPERIMENT

2.1. Instruments. The morphology of ZnO nanorods is studied using an ULTRA 55 field-emission scanning electron microscopy (FE-SEM) system (Karl Zeiss). A Perkin−Elmer Lambda 35 device is used to measure the UV-visible spectra of the self-assembled structures. An X-Pert PRO, PANalytical X-ray diffractometer, which uses Cu Kα radiation (λ = 1.54056 Å), is used to obtain the diffractograms (XRD) of the ZnO nanorods.

X-ray photoelectron spectroscopy (XPS) for ZnO rods are carried out using Axis Ultra DLD manufactured by Kratos Analytical UK. The radiation used is Al Kα (1.486 keV). Calibration is done using the C 1S electron peak, which occurs at 284.8 eV. Contact angle is measured using Holmarc contact angle meter (Model No. HO-IAD-CAM-01).

The height of the ZnO nanorods is determined using a Bruker surface profiler (Dektak XT). The current density−voltage (J−V) characteristics of the fabricated OPVs are measured using a Keithley Model 4200 parameter analyzer under simulated solar light irradiation. Oriel Sol3A Class AAA solar simulators are used in this experiment. The air mass (AM) chosen is 1.5. The fabricated devices have an active area of 1 mm^2. For the J−V measurements, a light intensity of 1 kW m^{-2} is employed. The intensities are calibrated using a standard Si solar cell.

Fabrication of the OPV is carried out inside a Jacomex glovebox (GP II P T2); a nitrogen atmosphere is maintained within the glovebox. The metal evaporation for fabricating the electrodes is carried out using thermal evaporator integrated with a glovebox (Angstrom Engineering, Nexdep).

2.2. Synthesis of ZnO Nanorods. The synthesis of ZnO nanorods involves nucleation followed by controlled growth of the rods.[29] The nanorods are seeded on an ITO-coated glass substrate using an equimolar mixture of 10 mM zinc acetate dehydrate (Zn $(CH_3COO)_2{\cdot}2(H_2O)$ (99%, SD fine) and hexamethylenetetramine (HMTA (99.5%, SD fine)). The mixture is prepared in ethanol solvent. This solution is spin-coated on a clean glass substrate at 500 rpm for 60 s. This procedure is repeated five times to ensure the seed layer is uniformly coated on the surface. A hot plate is maintained at 300 °C. Spin-coated substrates are placed on the hot plate and annealed isothermally for 1 h to form a ZnO seed layer. This is the seeding method used for both growth approaches explored (see below),.

ZnO nanorods are grown on the seed-layer-coated substrates. An equimolar mixture of $Zn(NO_3)_2{\cdot}6H_2O$ (99.99%, Aldrich) and HMTA in deionized (DI) water is used as the growth medium. The concentrations of the precursors are varied (5, 20, and 50 mM) in order to modify the aspect ratios of the ZnO nanorods. The ZnO nanorod growth is performed on these seeded substrates using two different approaches:

(i) The seeded substrates described above are immersed in the growth medium at 85 °C for 1 h. The substrate is placed at the bottom of the chemical bath with the seed layer facing upward as shown in Figure 2. This sample is labeled as $ZnO_{nanorods\text{-}upward}$.

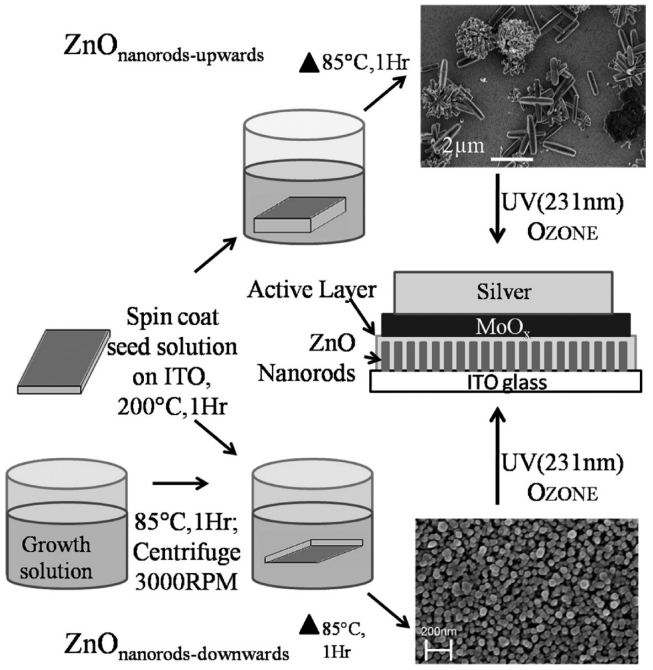

Figure 2. Schematic representation of the growth procedures adopted for the ZnO nanorods.

(ii) Before growing the ZnO nanorods on the seed layer, the growth medium is heated to 85 °C for 1 h. After which we centrifuge the solution at 3000 rpm for 20 min. The centrifuged solution is collected and used as the growth solution. This process is done to remove unwanted precipitates of ZnO. In the absence of the preheating and centrifugation, precipitates would settle on the substrate and induce inhomogeneities in the ZnO layer.

The substrate is fixed to a fixture such that, when immersed and suspended in the growth solution, the seed layer faces downward, as shown in Figure 2. The growth medium is heated to 85 °C for 1 h for the ZnO nanorods; the growth occurs on the seed layer. In this manuscript, the material formed using this method is referenced as $ZnO_{nanorods\text{-}downward}$.

The as-grown samples are thoroughly rinsed in deionized (DI) water. This rinsing is followed by drying using a nitrogen gun. The resulting samples are subjected to UV-ozone treatment for various intervals of time.[30]

2.3. Device Fabrication. ITO substrates (70−150 $\Omega\ \square^{-1}$; Delta Technologies) are cleaned thoroughly by sonicating them using acetone, DI water, soap solution (5% labolene solution), DI water, and isopropyl alcohol (IPA). Each of these sonication steps is done over 5-min durations. The cleaned substrates are dried using nitrogen gas.

On a clean and dry ITO substrate, a ZnO nanorod layer is grown using the procedure mentioned above ($ZnO_{nanorods\text{-}upward}$ and $ZnO_{nanorods\text{-}downward}$). UV-treated samples are immediately

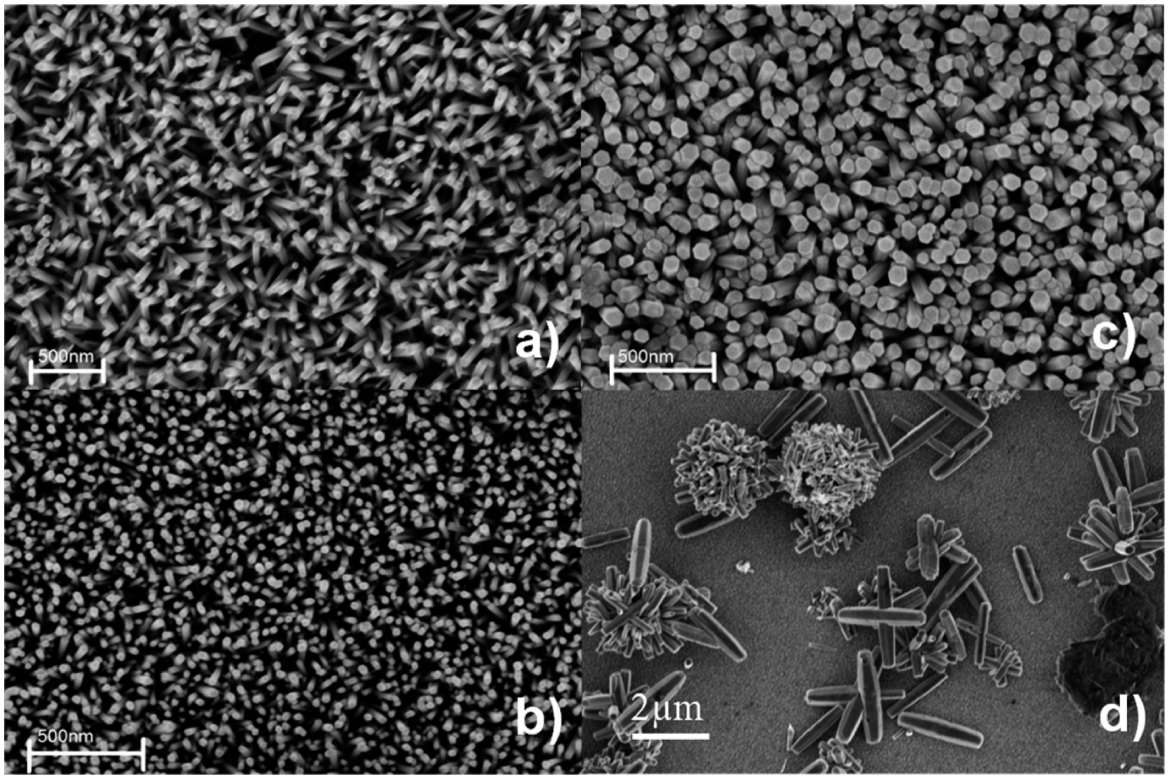

Figure 3. SEM of (a−c) $ZnO_{nanorods\text{-}upward}$ grown over 1 h using 5, 20, and 50 mM zinc nitrate solutions, and (d) lateral heterogeneities on the sample.

transferred into the glovebox in order to avoid any possibility of contamination.

Inside the glovebox, a mixture of poly-3-hexylthiophene-2,5-diyl (P3HT from Rieke Metals, Catalog No. 4002-EE), and phenyl-C61-butyric acid methyl ester (PCBM, Nano-C) is prepared. Both P3HT and PCBM are mixed in dichlorobenzene (DCB) solvent. In 1 mL of DCB, 7.5 mg each of P3HT and PCBM are dissolved. The required dissolution requires overnight (∼12 h) stirring. The P3HT:PCBM mixture is spin-coated on the ZnO nanorod containing substrate (at 1000 rpm for a duration of 60 s). Typically, for a single device, 150 μL of the solution is used. The fabricated heterostructure is annealed for 15 min at 150 °C on a hot plate.[31] This aids in the phase separation of P3HT and PCBM, which, in turn, helps in establishing a well-functioning bulk heterojunction.[32,33] The device that uses the 5 mM growth solution for growing ZnO nanorods is labeled $device_{5\ mM}$. Devices grown using the 20 mM and 50 mM solutions are labeled as $device_{20\ mM}$ and $device_{50\ mM}$, respectively

Thermal deposition of the hole transport (i.e., MoO_3, Aldrich, Lot No. 203815, 99.99% pure) and anode (Ag, Lot No. 12186, Alfa Aesar) layers is carried out at 1×10^{-6} Torr. During the process optimization stage, we focused on a 1 mm^2 physical mask. To maintain consistency, we fabricate devices using 1 mm^2 active area. During deposition the substrate is rotated at a constant rate. Molybdenum trioxide (MoO_3, 5 nm thickness) is deposited at a rate of 0.5 Å/s. Ag is thermally deposited at 0.5 Å/s during the first 20 nm, after which the rate is increased to 1 Å/s. The overall thickness of the Ag anode is ∼100 nm.

3. RESULTS AND DISCUSSION

3.1. Structural and Morphological Characterization. $ZnO_{nanorods\text{-}upward}$ is grown with increasing concentrations (i.e., from 5 mM to 50 mM), which results in an increasing diameter of the ZnO nanorods (20 ± 4 nm to 60 ± 12 nm), as shown in Figure 3. We observe that the spatial density of nanorods steadily increases with growth solution concentration. The total surface area of the $ZnO_{nanorods\text{-}upward}$ depends on (i) its height, (ii) its cross-sectional area, and (iii) its areal density. Using a profilometer, the height of the nanorods is determined to be ∼65 nm. Image processing using ImageJ software is used to determine the average cross-sectional area of the nanorods and the areal nanorod density.[34,35] We find that ZnO nanorods grown over a substrate area of 1 μm^2 have a total surface area of 1.81 ± 0.15 μm^2 and 1.65 ± 0.18 μm^2, when the growth concentrations are 20 and 50 mM, respectively. However, from Figure 3d, we also notice that there exists heterogenities in the $ZnO_{nanorods\text{-}upward}$, which is clearly not desirable.

$ZnO_{nanorods\text{-}downward}$ is grown using growth solutions with concentrations varying over a range of 10−50 mM. This results in nanorods with diameters varying from 35 ± 15 nm to 70 ± 25 nm (Figure 4). Figure 4c shows that the rods are merged and very dense. There is a steady increase in the density of rods with increasing concentration of the growth solution. We find that the ZnO nanorods grown over a substrate area of 1 μm^2 have a total surface area of 1.62 ± 0.12 μm^2 and 1.78 ± 0.13 μm^2, when the growth concentrations are 10 and 20 mM, respectively. Hence, the interfacial area over which electron collection is performed increases by 65%−80% when nanorods are used. This area is calculated using the assumption that all rods grow with a hexagonal habit (this is reasonable, since the ZnO that is grown has the wurtzite crystal structure).[36]

Figure 5a shows the XRD pattern of $ZnO_{nanorods\text{-}upward}$. This sample has the wurtzite crystal structure (space group $P6_3mc$). The characteristic peaks observed are (100), (002), (101), and (110). In addition to the (002) peak, the presence of other

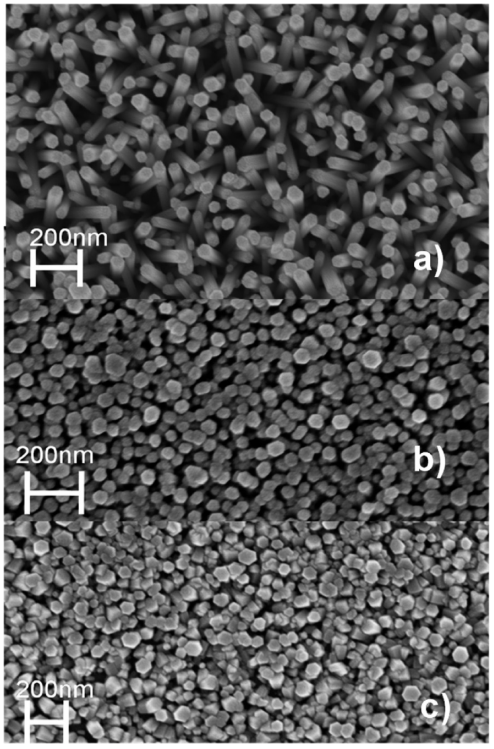

Figure 4. SEM images of $ZnO_{nanorods\text{-}upward}$ grown over 1 h using (a) 5 mM, (b) 20 mM, and (c) 50 mM zinc nitrate solutions.

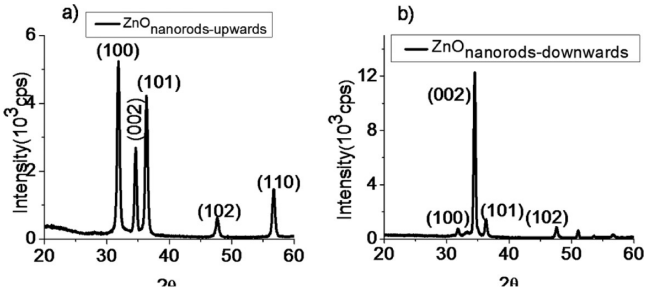

Figure 5. XRD patterns of (a) $ZnO_{nanorods\text{-}upward}$ and (b) $ZnO_{nanorods\text{-}downward}$ on ITO-coated glass substrate.

peaks suggest that all the rods are not perfectly oriented along the (002) direction. Clearly, this is one of the sources of lateral heterogeneities in this sample.

Figure 5b shows the XRD pattern of $ZnO_{nanorods\text{-}downward}$. The pattern observed is consistent with JCPDS File Card No. 01-079-0206. The ZnO (002) peak at $2\theta \approx 34°$ is observed, revealing that the films have the wurtzite crystal structure (space group $P6_3mc$). In this sample, the nanorods are significantly oriented along the *c*-axis (which is perpendicular to the substrate), which is also consistent with the results obtained by SEM analysis. The electron mobility of ZnO is highest along the (002) direction;[37] this is due to the corresponding effective mass being low. Given this fact, the observed orientation makes $ZnO_{nanorods\text{-}downward}$ very desirable as an electron collector (cathode).[38,39] The investigation concerning the reason underlying the significant homogeneity of $ZnO_{nanorods\text{-}downward}$ is currently being pursued.

3.2. Ultraviolet−Visible/Transmission Studies. Figure 6 shows UV-vis spectra of UV-ozone treated (treatment time ≈ 5−30 min) of $ZnO_{nanorods\text{-}downward}$ (grown for 1−5 h duration). These samples are grown using the 20 mM growth solution. As

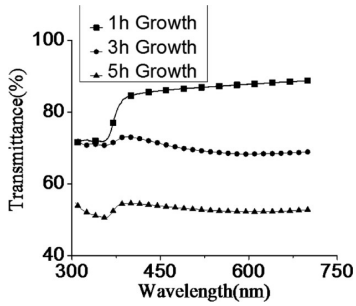

Figure 6. UV-vis spectra of UV-ozone treated $ZnO_{nanorods\text{-}downward}$ (grown over varying durations).

the growth time increases, the height of the rods increases. For samples grown for 1 and 5 h, the observed heights of the rods are ∼55 nm and ∼150 nm, respectively.[40] Increasing the height of the ZnO nanorods leads to an increase in optical loss, because of scattering, which, in turn, results in a reduction in transmittance. Samples containing ZnO nanorods grown for 1 h exhibit the highest transmittance (∼85%, averaged over solar spectrum) and, hence, are used to fabricate OPV.

3.3. Contact Angle Measurements. To understand the effect of surface treatment on the device properties, contact angle measurements are carried out using DCB droplets on $ZnO_{nanorods\text{-}downward}$ samples (with and without UV ozone treatment). When compared to untreated ZnO nanorods, UV-ozone treated nanorods exhibit a decrease in contact angle for both in DCB (Figure 7). This suggests that there is an

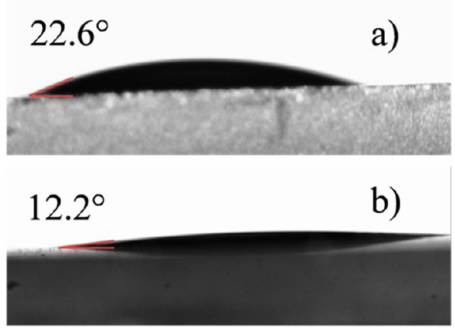

Figure 7. Contact angle measurement shows a decrease in contact angle in UV-ozone treated ZnO. The figure shows a droplet (volume = 2 mL) of DCB on (a) untreated and (b) UV-ozone treated $ZnO_{nanorods\text{-}downward}$ sample.

improvement in wettability of UV-ozone treated surfaces. Because of the better wettability of the UV-ozone treated samples, a better interface between the active components and the ZnO nanorods is possible using these systems.[41,42]

3.4. X-ray Photoelectron Spectroscopy. For both the $ZnO_{nanorods\text{-}downward}$ and $ZnO_{nanorods\text{-}upward}$ samples, the XPS results are similar. We present the representative data here. XPS spectra for C 1s, O 1s, and Zn 2p are measured for as-prepared $ZnO_{nanorods\text{-}downward}$, and for UV-ozone treated samples. The C 1s electron peak (at 284.6 eV) is used for calibration of the binding energies. For untreated samples, two distinct O 1s (Figure 8a) peaks appear, at ∼531.3 and ∼534.3 eV. These peaks are attributed to oxygen in ZnO and oxygen in surface hydroxyls, respectively. UV-ozone treatment increases the relative magnitude of the peak at ∼531.3 eV; the peak at ∼534.3 eV diminishes in intensity. This suggests a decrease in

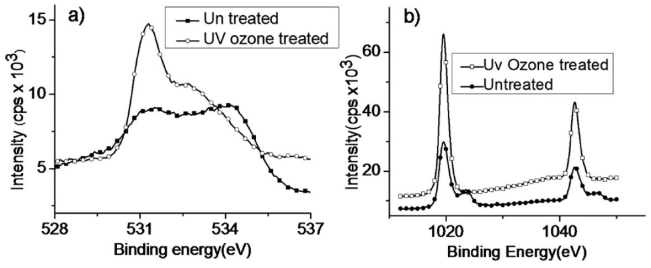

Figure 8. XPS peak analysis for $ZnO_{nanorods\text{-}downward}$: (a) O 1s and (b) Zn 2p.

the concentration of surface hydroxyls in the UV-ozone treated samples. The increase in the intensity of the ~531.3 eV peak in UV-ozone-treated samples indicates an increase in the amount of O−Zn bonds at the ZnO surface.[44] Hence, during the UV-ozone treatment, several oxygen vacancies are passivated.

The Zn $2p_{3/2}$ and Zn $2p_{1/2}$ peaks (Figure 8b) are observed at 1019.2 and 1042.2 eV, respectively. The Zn $2p_{3/2}$ spectra peaked at ~1019.24 eV, which can be attributed to the formation of ZnO.[43] The intensity of both Zn 2p peaks, which corresponds to the Zn−O bonds,[44−46] increases after UV-ozone treatment. This increase in intensity is consistent with the trend observed for O 1s spectra.

In short, XPS studies reveal that UV-ozone treatment results in (i) a decrease in the concentration of surface hydroxyls, and (ii) an increase in the concentration of Zn−O surface bonds, both of which are desirable.

3.5. Device Characterization. Given the discussion in section 3.1, we expect heterogeneities in $ZnO_{nanorods\text{-}upward}$ to yield devices that have significant leakages and short-circuit current pathways between the electrodes. This is consistent with what we observe ($J-V$ characteristics of $ZnO_{nanorods\text{-}upward}$ are shown in Figure 9). The short-circuit current density (J_{sc})

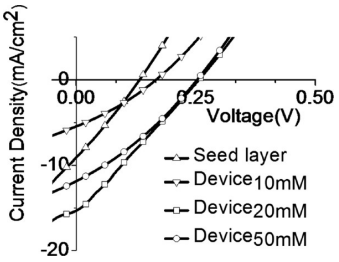

Figure 9. Current density−voltage ($J-V$) characteristics of I-OPV fabricated using $ZnO_{nanorods\text{-}upward}$.

and open-circuit voltages (V_{oc}) are tabulated in Table 1. Better performance is observed for $device_{20\ mM}$ (efficiency of ~1.2%). On the other hand, $device_{50\ mM}$ shows lower efficiency (~0.32%). The devices fabricated using the reported protocol exhibit significantly lower V_{oc} values. This could be due to the

Table 1. Characteristics of Devices Made Using $ZnO_{nanorods\text{-}upwards}$, Grown Using Solutions of Various Growth Concentrations

$ZnO_{nanorods\text{-}upward}$	J_{sc}(mA/cm^2)	V_{oc}(V)	fill factor, FF (%)	η (%)
only seed layer	5.45	0.16	36	0.27
$device_{5\ mM}$	9.1	0.133	26.9	0.32
$device_{20\ mM}$	15.4	0.257	26	1.03
$device_{50\ mM}$	11.9	0.25	39	0.92

leakages caused by lateral heterogeneities (recall Figure 3d) in the device and it also could be due to inefficient wetting of the active material on ZnO.

$J-V$ characteristics of $ZnO_{nanorods\text{-}downward}$ are shown in Figure 10, and the short-circuit current density (J_{sc}) and open-circuit

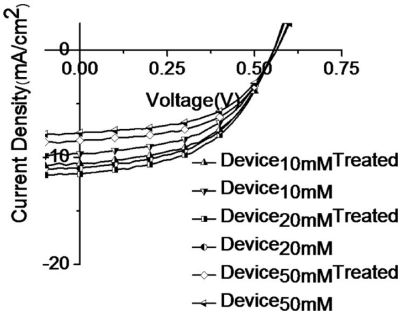

Figure 10. $J-V$ characteristics of I-OPV fabricated using $ZnO_{nanorods\text{-}downward}$.

Table 2. Characteristics of Devices Made Using $ZnO_{nanorods\text{-}downward}$, Grown Using Solutions of Various Growth Concentrations

$ZnO_{nanorods\text{-}downward}$	J_{sc} (mA/cm^2)	V_{oc} (V)	fill factor, FF (%)	η (%)
$device_{10\ mM}$	10.59	0.56	0.50	2.96
$device_{10\ mM}$, treated	9.67	0.56	0.50	2.71
$device_{20\ mM}$	11.04	0.56	0.49	3.06
$device_{20\ mM}$, treated	11.59	0.56	0.49	3.21
$device_{50\ mM}$	8.44	0.58	0.51	2.50
$device_{50\ mM}$, treated	7.71	0.58	0.51	2.28

voltages (V_{oc}) are tabulated in Table 2. The short-circuit current density in these devices is on the lower side, but these devices show significantly better performance than $ZnO_{nanorods\text{-}upward}$-based devices. Also, the open-circuit voltage (V_{oc}) is reasonable. Better V_{oc} and overall performance of these devices is attributed to the improved texture and increased lateral homogeneity of the ZnO nanorods. Hereafter, the devices described use $ZnO_{nanorods\text{-}downward}$.

The improved device performance of $device_{20\ mM}$ is attributed to enhanced interface area. We also observe that $device_{50\ mM}$ and $device_{10\ mm}$ have lower current densities, which is due to the low density of ZnO nanorods in these samples (which, in turn, results in low ZnO-organic interfacial area). This is consistent with SEM image analysis (discussed earlier), wherein it is noted that the 20 mM growth solution results in relatively uniform ZnO nanorods and a higher surface area. Hence, $device_{20\ mM}$ (fabricated on $ZnO_{nanorods\text{-}downward}$) is chosen for further study.

We also observe that $device_{20\ mM}$ performs as well as it does (at least partially) because of improved wetting characteristics of DCB on UV-ozone-treated ZnO (see Figure 7). In fact, the high current density observed in $device_{20\ mM}$ (~11.5 mA cm^{-2}) is very encouraging (Figure 10) and is attributed to the high surface area of the nanorods; this, in turn, results in better electron collection efficiency.[47] In addition, $device_{20\ mM}$ consistently shows a similar trend of high current density and significantly improved V_{oc} values, leading to overall improved efficiency of the device; this is reasonable, given the homogeneity of the $ZnO_{nanorods\text{-}downward}$ samples. Hence, the

process reported here to fabricate device$_{20\ mM}$ is very reliable and reproducible.

4. CONCLUSIONS

Two different soft-chemical solution-growth methods are developed to fabricate self-assembled, oriented ZnO nanorods, which are subsequently used for electron collection in an inverted OPV device. Substrate mounting, surface properties, and optical transmittance are optimized by varying the nanorod growth conditions, and by employing UV- ozone treatment. XRD analysis suggests that the grown ZnO$_{nanorods\text{-}upward}$ have lateral heterogeneities (i.e., these nanorods are not completely textured). However, ZnO$_{nanorods\text{-}downward}$ does not have lateral heterogeneities; in fact, these nanorods are all almost uniformly oriented in the (002) direction, which is the preferred direction for use in applications related to electron collection.

Contact angle measurements suggest improved wettability of DCB on UV-ozone treated ZnO$_{nanorods\text{-}downward}$ films. The change in surface chemistries of the ZnO nanorods, before and after the treatment, is understood using XPS. We show that UV-ozone-treated ZnO$_{nanorods\text{-}downward}$ results in a much better interface between the active layer and the ZnO nanorods, which, in turn, translates to better devices, with an efficiency of 3.2% and a fill factor (FF) of 50%, with a short circuit density of 11.6 mA cm^{-2}.

In short, UV-ozone-treated ZnO$_{nanorods\text{-}downward}$ show an improvement in optical transmission, increased wetting of active components mixture, decreased concentration of surface hydroxyls, and an increased concentration of Zn−O surface bonds, all of which correlate well with improved device performance.

AUTHOR INFORMATION

Corresponding Authors

*Tel.: (+91) 802-293-2515. E-mail: tt332@cornell.edu (T. Thomas).

*Tel.: (+91)80-2293-2467. E-mails: praveen@materials.iisc.ernet.in, onegroupb203@gmail.com (P. C. Ramamurthy).

Notes

The authors declare no competing financial interest.

ACKNOWLEDGMENTS

This work is based upon work supported in part under the U.S.−India Partnership to Advance Clean Energy-Research (PACE-R) for the Solar Energy Research Institute for India and the United States (SERIIUS), funded jointly by the U.S. Department of Energy (Office of Science, Office of Basic Energy Sciences, and Energy Efficiency and Renewable Energy, Solar Energy Technology Program, under Subcontract No. DE-AC36-08GO28308 to the National Renewable Energy Laboratory, Golden, CO) and the Government of India, through the Department of Science and Technology under Subcontract IUSSTF/JCERDC-SERIIUS/2012 dated Nov. 22, 2012. Dr. Tiju Thomas acknowledges support received from Department of Science &Technology (Govt. of India), through Grant No. DST 01117.

REFERENCES

(1) He, Z.; Zhong, C.; Su, S.; Xu, M.; Wu, H.; Cao, Y. Enhanced Power-Conversion Efficiency in Polymer Solar Cells Using an Inverted Device Structure. *Nat. Photonics* **2012**, *6*, 591−595.

(2) Chen, H.-Y.; Hou, J.; Zhang, S.; Liang, Y.; Yang, G.; Yang, Y.; Yu, L.; Wu, Y.; Li, G. Polymer Solar Cells with Enhanced Open-Circuit Voltage and Efficiency. *Nat. Photonics* **2009**, *3*, 649−653.

(3) Liang, Y.; Xu, Z.; Xia, J.; Tsai, S.-T.; Wu, Y.; Li, G.; Ray, C.; Yu, L. For the Bright Future—Bulk Heterojunction Polymer Solar Cells with Power Conversion Efficiency of 7.4%. *Adv. Mater.* **2010**, *22*, E135−E138.

(4) Kawano, K.; Pacios, R.; Poplavskyy, D.; Nelson, J.; Bradley, D. D. C.; Durrant, J. R. Degradation of Organic Solar Cells Due to Air Exposure. *Sol. Energy Mater. Sol. Cells* **2006**, *90*, 3520−3530.

(5) Deibel, C.; Dyakonov, V.; Brabec, C. Organic Bulk Heterojunction Solar Cells. *IEEE J. Sel. Top. Quantum Electron.* **2010**, *16*, 1517−1527.

(6) Kim, S.; Mor, G. K.; Paulose, M.; Varghese, O. K.; Shankar, K.; Grimes, C. A. Broad Spectrum Light Harvesting in TiO_2 Nanotube Array−Hemicyanine Dye−P3HT Hybrid Solid-State Solar Cells. *IEEE J. Sel. Top. Quantum Electron.* **2010**, *16*, 1573−1580.

(7) Şahin, Y.; Alem, S.; de Bettignies, R.; Nunzi, J.-M. Development of Air Stable Polymer Solar Cells using an Inverted Gold on Top Anode Structure. *Thin Solid Films* **2005**, *476*, 340−343.

(8) Sun, Y.; Takacs, C. J.; Cowan, S. R.; Seo, J. H.; Gong, X.; Roy, A.; Heeger, A. J. Efficient, Air-Stable Bulk Heterojunction Polymer Solar Cells Using MoO_x as the Anode Interfacial Layer. *Adv. Mater.* **2011**, *23*, 2226−2230.

(9) Catlow, C. R. A.; Sokol, A. A.; Walsh, A. Microscopic Origins of Electron and Hole Stability in ZnO. *Chem. Commun.* **2011**, *47*, 3386−3388.

(10) Jiang, W.-T.; Wu, C.-T.; Sung, Y.-H.; Wu, J.-J. Room-Temperature Fast Construction of Outperformed ZnO Nanoarchitectures on Nanowire-Array Templates for Dye-Sensitized Solar Cells. *ACS Appl. Mater. Interfaces* **2013**, *5*, 911−917.

(11) Ozgur, U.; Hofstetter, D.; Morkoc, H. ZnO Devices and Applications: A Review of Current Status and Future Prospects. *Proc. IEEE* **2010**, *98*, 1255−1268.

(12) Zhao, J.; Wang, A.; Green, M. A. 24.5% Efficiency Silicon PERT Cells on MCZ Substrates and 24.7% Efficiency PERL Cells on FZ Substrates. *Prog. Photovoltaics* **1999**, *7*, 471−474.

(13) Park, W. I.; Kim, J. S.; Yi, G.-C.; Bae, M. H.; Lee, H. Fabrication and Electrical Characteristics of High-Performance ZnO Nanorod Field-Effect Transistors. *Appl. Phys. Lett.* **2004**, *85*, 5052−5054.

(14) Hochbaum, A. I.; Yang, P. Semiconductor Nanowires for Energy Conversion. *Chem. Rev.* **2010**, *110*, 527−546.

(15) Zhao, S.-L.; Kan, P.-Z.; Xu, Z.; Kong, C.; Wang, D.-W.; Yan, Y.; Wang, Y. Electroluminescence of ZnO Nanorods/MEH-PPV Heterostructure Devices. *Org. Electron.* **2010**, *11*, 789−793.

(16) Hu, T.; Li, F.; Yuan, K.; Chen, Y. Efficiency and Air-Stability Improvement of Flexible Inverted Polymer Solar Cells Using ZnO/Poly(ethylene glycol) Hybrids as Cathode Buffer Layers. *ACS Appl. Mater. Interfaces* **2013**, *5*, 5763−5770.

(17) Meng, X.; Shi, Z.; Chen, X.; Zeng, X.; Fu, Z. Temperature Behavior of Electron-Acceptor Transitions and Oxygen Vacancy Recombinations in ZnO Thin Films. *J. Appl. Phys.* **2010**, *107*, 023501.

(18) Tam, K. H.; Cheung, C. K.; Leung, Y. H.; Djurišić, A. B.; Ling, C. C.; Beling, C. D.; Fung, S.; Kwok, W. M.; Chan, W. K.; Phillips, D. L.; Ding, L.; Ge, W. K. Defects in ZnO Nanorods Prepared by a Hydrothermal Method. *J. Phys. Chem. B* **2006**, *110*, 20865−20871.

(19) Bai, W.; Yu, K.; Zhang, Q.; Xu, F.; Peng, D.; Zhu, Z. Large-Scale Synthesis of ZnO Flower-Like and Brush Pen-like Nanostructures by a Hydrothermal Decomposition Route. *Mater. Lett.* **2007**, *61*, 3469−3472.

(20) Wang, J.; Gao, L. Synthesis of Uniform Rod-Like, Multi-Pod-Like ZnO Whiskers and their Photoluminescence Properties. *J. Cryst. Growth* **2004**, *262*, 290−294.

(21) Chen, D.-W.; Wang, T.-C.; Liao, W.-P.; Wu, J.-J. Room-Temperature Fast Construction of Outperformed ZnO Nanoarchitectures on Nanowire-Array Templates for Dye-Sensitized Solar Cells. *ACS Appl. Mater. Interfaces* **2013**, *5*, 8359−8365.

(22) Yang, P.; Yan, H.; Mao, S.; Russo, R.; Johnson, J.; Saykally, R.; Morris, N.; Pham, J.; He, R.; Choi, H.-J. Controlled Growth of ZnO

Nanowires and Their Optical Properties. *Adv. Funct. Mater.* **2002**, *12*, 323−331.
(23) Yin, Z.; Liu, X.; Yao, H.; Wu, Y.; Hao, X.; Han, M.; Xu, X. Light Extraction Enhancement of GaN LEDs by Hybrid ZnO Micro-Cylinders and Nanorods Array. *IEEE Photonics Technol. Lett.* **2013**, *25*, 1989−1992.
(24) Neal, J. S.; Giles, N. C.; Yang, X.; Wall, R. A.; Ucer, K. B.; Williams, R. T.; Wisniewski, D. v.; Boatner, L. A.; Rengarajan, V.; Nause, J.; Nemeth, B. Evaluation of Melt-Grown, ZnO Single Crystals for Use as Alpha-Particle Detectors. *IEEE Trans. Nucl. Sci.* **2008**, *55*, 1397−1403.
(25) Vayssieres, L.; Keis, K.; Hagfeldt, A.; Lindquist, S.-E. Three-Dimensional Array of Highly Oriented Crystalline ZnO Microtubes. *Chem. Mater.* **2001**, *13*, 4395−4398.
(26) Vayssieres, L. Growth of Arrayed Nanorods and Nanowires of ZnO from Aqueous Solutions. *Adv. Mater.* **2003**, *15*, 464−466.
(27) Sarkar, K.; Rawolle, M.; Herzig, E. M.; Wang, W.; Buffet, A.; Roth, S. V.; Müller-Buschbaum, P. Custom-Made Morphologies of ZnO Nanostructured Films Templated by a Poly(styrene-block-ethylene oxide) Diblock Copolymer Obtained by a Sol−Gel Technique. *ChemSusChem* **2013**, *6*, 1414−1424.
(28) Orilall, M. C.; Wiesner, U. Block Copolymer based composition and morphology control in nanostructured hybrid materials for Energy Conversion and Storage, Solar Cells, Batteries, and Fuel Cells. *Chem. Soc. Rev.* **2011**, *40*, 520−535.
(29) Boyle, D. S.; Govender, K.; O'Brien, P. Novel Low Temperature Solution Deposition of Perpendicularly Orientated Rods of ZnO: Substrate Effects and Evidence of the Importance of Counter-Ions in the Control of Crystallite Growth. *Chem. Commun.* **2002**, 80−81.
(30) Ju, S.; Lee, K.; Yoon, M.-H.; Facchetti, A.; Marks, T. J.; Janes, D. B. High Performance ZnO Nanowire Field Effect Transistors with Organic Gate Nanodielectrics: Effects of Metal Contacts and Ozone Treatment. *Nanotechnology* **2007**, *18*, 155201.
(31) Ma, W.; Yang, C.; Gong, X.; Lee, K.; Heeger, A. J. Thermally Stable, Efficient Polymer Solar Cells with Nanoscale Control of the Interpenetrating Network Morphology. *Adv. Funct. Mater.* **2005**, *15*, 1617−1622.
(32) Yang, X.; Loos, J. Toward High-Performance Polymer Solar Cells: The Importance of Morphology Control. *Macromolecules* **2007**, *40*, 1353−1362.
(33) Hoppe, H.; Sariciftci, N. S. Morphology of Polymer/Fullerene Bulk Heterojunction Solar Cells. *J. Mater. Chem.* **2006**, *16*, 45−61.
(34) Abràmoff, M. D.; Magalhães, P. J.; Ram, S. Image Processing with ImageJ. *J. Biophotonics Int.* **2004**, *11*, 36−42.
(35) Thomas, T.; Chatman, S.; Wells, J.; Eberley, L.; Rasheed, M. A.; Poduska, K. M. Lateral Heterogeneities in ZnO Electrodeposits and Their Impact on Electrical and Optical Properties. *ECS Solid State Lett.* **2012**, *1*, P35−P37.
(36) Govender, K.; Boyle, D. S.; Kenway, P. B.; O'Brien, P. Understanding the Factors that Govern the Deposition and Morphology of Thin Films of ZnO from Aqueous Solution. *J. Mater. Chem.* **2004**, *14*, 2575−2591.
(37) Zhukov, V. P.; Echenique, P. M.; Chulkov, E. V. Two Types of Excited Electron Dynamics in Zinc Oxide. *Phys. Rev. B* **2010**, *82*, 094302.
(38) Fortunato, E.; Barquinha, P.; Pimentel, A.; Gonçalves, A.; Marques, A.; Pereira, L.; Martins, R. Recent Advances in ZnO Transparent Thin Film Transistors. *Thin Solid Films* **2005**, *487*, 205−211.
(39) Ong, B. S.; Li, C.; Li, Y.; Wu, Y.; Loutfy, R. Stable, Solution-Processed, High-Mobility ZnO Thin-Film Transistors. *J. Am. Chem. Soc.* **2007**, *129*, 2750−2751.
(40) Guo, M.; Diao, P.; Cai, S. Hydrothermal Growth of Well-Aligned ZnO Nanorod Arrays: Dependence of Morphology and Alignment Ordering upon Preparing Conditions. *J. Solid State Chem.* **2005**, *178*, 1864−1873.
(41) Kwak, G.; Seol, M.; Tak, Y.; Yong, K. Superhydrophobic ZnO Nanowire Surface: Chemical Modification and Effects of UV Irradiation. *J. Phys. Chem. C* **2009**, *113*, 12085−12089.
(42) Beek, W. J. E.; Wienk, M. M.; Kemerink, M.; Yang, X.; Janssen, R. A. J. Hybrid Zinc Oxide Conjugated Polymer Bulk Heterojunction Solar Cells. *J. Phys. Chem. B* **2005**, *109*, 9505−9516.
(43) Ju, S.; Lee, K.; Yoon, M.-H.; Facchetti, A.; Marks, T. J.; Janes, D. B. High Performance ZnO Nanowire Field Effect Transistors with Organic Gate Nanodielectrics: Effects of Metal Contacts and Ozone Treatment. *Nanotechnology* **2007**, *18*, 155201.
(44) Du, T.; Ilegbusi, O. J. Synthesis and Morphological Characterization on PVP/ZnO Nano Hybrid Films. *J. Mater. Sci.* **2004**, *39*, 6105−6109.
(45) Lv, Y.; Yu, L.; Huang, H.; Feng, Y.; Chen, D.; Xie, X. Application of the Soluble Salt-Assisted Route to Scalable Synthesis of ZnO Nanopowder with Repeated Photocatalytic Activity. *Nanotechnology* **2012**, *23*, 065402.
(46) Deng, D.; Martin, S. T.; Ramanathan, S. Synthesis and Characterization of One-Dimensional Flat ZnO Nanotower Arrays as High-Efficiency Adsorbents for the Photocatalytic Remediation of Water Pollutants. *Nanoscale* **2010**, *2*, 2685−2691.
(47) Kwon, S.; Shim, M.; Lee, J. I.; Lee, T.-W.; Cho, K.; Kim, J. K. Ultrahigh Density Array of CdSe Nanorods for CdSe/Polymer Hybrid Solar Cells: Enhancement in Short-Circuit Current Density. *J. Mater. Chem.* **2011**, *21*, 12449−12453.